

Real-time monitoring of pulsed cavitation ultrasound therapy using coherent passive cavitation imaging: perspectives for volumetric imaging

Daniel Suarez Escudero^{1,2}, Mickael Tanter¹, Mathieu Pernot¹

¹Physics for Medicine Paris, Inserm U1273, ESPCI Paris, CNRS FRE 2031, PSL University, 17 rue Moreau, 75012 Paris, France

²Cardiawave SA, 29 rue du Faubourg Saint Jacques, 75014, Paris, France

Abstract—Pulsed cavitation ultrasound therapies (PCUT) such as histotripsy are non-invasive therapeutic approaches effective in various medical indications, relying on the mechanical effects generated by inertial cavitation bubbles. Even though limited by the poor contrast, conventional ultrasound B-Mode imaging has been widely used for the guidance and monitoring of the therapeutic procedure, allowing the visualization of the cavitation bubble cloud. However, B-Mode imaging lacks specificity and the visualization of the bubble cloud is often limited in deep and moving organs such as the liver and the heart and remains moreover subjective for the operator. We previously developed a new imaging modality to better identify the cavitation cloud based on a coherent passive ultrasound imaging approach combined with a spatiotemporal filter to map the bubble cloud with high sensitivity and high contrast. Yet, 2D imaging is limited as the therapeutic focal spot is constrained to be located inside the imaging plane, which is an engineering challenge as there might be mechanical misalignments between both the therapy and the imaging transducers as well as ultrasound aberrations leading to monitoring failure. We propose to extend the technique to volumetric imaging, allowing to overcome these limitations, and to explore its performances on an aberrated beam.

Keywords—*histotripsy, cavitation, passive cavitation imaging, ultrasound therapy, real-time monitoring, volumetric ultrasound*

I. INTRODUCTION

Pulsed Cavitation Ultrasound Therapies (PCUT) such as histotripsy are based on inertial cavitation generated by the high-intensity ultrasound emission from a transducer. Ultrasound is focused at a specific focal spot (geometrically and/or electronically) and the strong negative pressures at this spot will cause bubbles to nucleate [1][2].

Such therapies are currently guided mostly by conventional ultrasound B-Mode imaging, which allows a visualization of both the anatomic structures and the bubble cloud inside a two-dimensional imaging plane [1][2]. Nevertheless, B-Mode imaging lacks specificity and the effective visualization of the bubble cloud depends strongly on the image quality, and the low contrast of B-Mode images remains an important limitation for applications in deep organs such as the heart or the liver. In fact, it is not often clear where the bounds of the bubble cloud are and, as bubbles are generated inside heterogenic biological tissues, their echoes are difficult to discriminate, and the visualization of the bubble cloud remains subjective and qualitative for the operator.

For now, several 2D cavitation imaging techniques have been developed for PCUT monitoring, allowing to beamform a 2D slice of the bubble cloud which leads to an overview of its size, shape and location [3]. From a technical point of view, those imaging methods often impose the cavitation cloud to be inside the imaging plane, and thus there is an engineering challenge to precisely interlock the imaging probe and the therapy transducer and to maintain the position during the whole procedure. A misalignment between both transducers could lead to a misfire and cavitation would be nucleated outside the imaging plane.

Moreover, independently from the pure mechanical alignment, ultrasound beams could be distorted by aberration layers and nucleation could also happen out-of-plane. Indeed, if the propagation medium is heterogenic and in particular if it contains strong reflectors or strong interfaces such as the ribs or fatty tissues, the therapeutic ultrasound field can be aberrated with potential major effects such as:

- Distortion of the focal spot shape;
- Displacement of the focal spot from its intended position, and in particular outside the imaging plane;
- Creation of secondary focal spots, leading to secondary cavitation clouds nucleation.

Impeding the visualization of the cloud(s) and resulting in a critical security risk for the patient.

Cavitation is a three-dimensional phenomenon, and a 2D monitoring is limited in the way that we can only supervise a slice of the cloud, ignoring its full shape and thus the possible target tissues around a three-dimensional volume surrounding the focal spot.

We proposed a 3D imaging method based on coherent passive cavitation imaging [4] allowing to image the entire sonicated volume and thus to image the whole cavitation cloud, even if it is located outside the central axis of the therapy transducer. The approach is based on pulse-echo imaging of the high intensity pulse transmitted by a large focused transducer and received on a matrix array probe embedded in the therapeutic transducer. A spatiotemporal singular value decomposition is used to filter out the bubble signal from the backscattered tissue echoes with high contrast. We investigated this approach *in vitro* through a layer of human ribs.

II. MATERIAL AND METHODS

A. Experimental setup

We used a 700 kHz focused therapy transducer ($f = 100$ mm, $f/D = 1$, Imasonic©, France) for high intensity ultrasound emissions, operated by a 2.5 kilo Watts power amplifier (RITEC©, USA) and we used a 32x32 matrix array (Vermon©, France) for 3D imaging. The probe was inserted in the central hole of the transducer (Figure 1) and fixed by a specifically conceived 3D printed support.

The therapy transducer driving signal was emitted by a function generator and consisted in a 700 kHz 8-cycle sine burst wave with a Pulse Repetition Frequency (PRF) of 100 Hz. For imaging, we used a customized, programmable, 1024-channel ultrasound system composed of 4 synchronized Vantage 256 (Verasonics©, USA) systems. The function generator was also intended as a master clock to trigger both the ultrasound scanner and the amplifier gate input.

The transducer was calibrated using an in-house optical heterodyne interferometer in water. The peak negative acoustic pressure was estimated to be approximately -9 MPa.

We placed 3 human ribs in front of the transducer to create an aberration on the therapeutic field and the whole was placed inside a tank filled with degassed water for cavitation generation in water. The imaging probe was positioned in between two ribs (Figure 1). It is to be noted that this configuration is close to an *in vivo* therapeutic cardiac procedure, where the imaging probe is placed between the intercostal spaces.



Figure 1 - Human ribs placed in front of the therapeutic transducer to create an aberration. The imaging probe was placed in an intercostal space (Vermon©, France).

B. Hydrophone measurements

Beforehand, we used a hydrophone (Onda©, HNC 400) connected to an amplifier and a scope to measure the pressure at the focus trough the ribs.

The hydrophone was moved by a 3D step motor stage, was placed at the focus of the transducer and the pressure was measured with and without the thoracic tissue inserted between the transducer and the hydrophone.

C. Passive acquisitions

We programmed passive imaging events where the imaging probe operated only as a receiver. All the 1024 elements were programmed to receive data and we acquired data with a 200% bandwidth using an IQ beamformer. The probe was centred at 3 MHz.

The Vantage systems and the therapy transducer were triggered simultaneously (rising edge) and the probe received data for 250 microseconds, which is the time needed to image about 20-centimeter depth at 1540 meters per second. No transmission occurs on the probe, and a burst of 8 cycles centred on 700 kHz was transmitted by the therapy transducer at each rising edge. The passive volume rate depended directly on the therapeutic burst emission frequency, which was set at 100 Hz in this study.

Passive data was beamformed by taking into account the reception delays and a global transmit delay [4][5] following a delay-and-sum algorithm, defining a synchronous transmit and receive sequence (pulse-echo). We used a CUDA optimized delay-and-sum algorithm incorporating absolute timing information. Each volume was reconstructed in post-processing after the whole 250 μ s of data was received, we acquired one volume after each therapeutic burst and the effective frame rate was 100 Hz. A time delay correction was included in the beamforming algorithm in order to allow the compensation of the spatial shift between the therapy transducer and the imaging probe for the coherent beamforming of the data.

The time delay was experimentally measured prior to the experiment in a water tank using a hydrophone placed at the focal point. It was measured as the difference of the arrival time of the signals emitted by the therapeutic transducer and by the imaging probe when focusing on the hydrophone.

D. Singular value decomposition filter and cavitation map

A clutter filter was applied to the data based on the Singular Value Decomposition (SVD) of data in space and time. This method has already been introduced for filtering ultrafast ultrasonic data and was applied to 2D cavitation imaging in moving organs [4] as it allows to efficiently cluster tissue and cavitation activity. It has been shown that the highest singular vectors correspond to tissue signal while cavitation activity, as it happens to be highly spatiotemporally incoherent, is within the lowest singular values. Moreover, as passive imaging only reconstructs the echoes of the therapeutic ultrasonic beam interactions with the medium, it avoids most of the clutter signals is effective in rapidly moving tissues.

The SVD is an algebraic decomposition technique of matrices. It adapts to local statistics in an image and maintains a maximum energy over a small amount of values. Briefly, it comes to factorizing a matrix $X_{m \times n}$ in the form:

$$X = U \cdot S \cdot V^* \quad (1)$$

where $U_{m \times m}$ is an orthogonal matrix, $V_{n \times n}$ is an orthogonal matrix and $S_{m \times n}$ is a diagonal matrix whose coefficients σ_i are the singular values of X . Please note that V^* is the conjugate transposed of V , and that the number of non-zero singular values of S is equal to the rank of X .

The challenge of the filtering remains the choice of the right singular vectors associated.

Let us consider a set of n_t passive volumes with dimensions n_x , n_y and n_z , where n_x , n_y and n_z are respectively the number

of spatial samples along the x , y and the z directions. The whole set can be rearranged in a space-time two-dimensional matrix form X ($n_x \times n_y \times n_z, n_t$), the Casorati Matrix. The singular value decomposition of this matrix consists in finding singular temporal and spatial vectors, respectively regrouped in the columns of two matrices U and V (see (2)). As seen, U and V are unitary matrices defining respectively the temporal and spatial singular vectors, arranged from the most energetic to the least energetic.

Next to the singular value decomposition (SVD) of the matrix X , it is about to reconstruct the volume using only the singular values which are relevant to the bubble cloud. We assume that the bubbles are described within a contiguous set of singular values. We then need to define the two boundary singular values p and q to finally obtain the specific bubble signals $X_{bubbles}$:

$$X_{bubbles}(n_x \times n_y \times n_z, n_t) = \sum_{i=p}^q \sigma_i U_i V_i^T \quad (2)$$

This new set can be rearranged in a four-dimensional matrix form $X_{bubbles}(n_x, n_y, n_z, n_t)$, and we can compute its power integral or cavitation map (CM), which is meant to map the most energetic areas of the image:

$$CM(n_x, n_y, n_z) = \int |X_{bubbles}(n_x, n_y, n_z, n_t)|^2 dt \quad (3)$$

Thus, n_t volumes will give one cavitation map, so the cavitation map will have a volume rate roughly divided by n_t compared to acquisition volume rate. Depending on the applications, it is important to optimize the number of volumes to use.

III. RESULTS

First, Figure 1 shows an example of a hydrophone pressure scan in water with and without the ribs following two orthogonal X and Y planes. In the Y plane through the ribs, we can observe a strong secondary lobe of about -3 dB below the main lobe, while secondary lobes remain low in the X plane with a difference of about 11 dB in relation to the main lobe. Without the ribs, the secondary lobes are about -11 dB below the main lobe in both planes. The attenuation coefficient of the ribs was estimated at $\alpha_{ribs} = 58 \pm 15\%$.

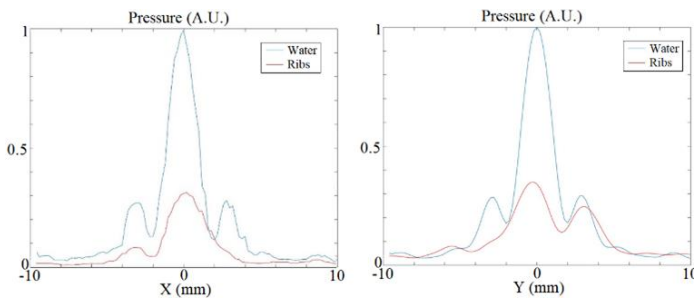


Figure 2 - Pressure scan in water with and without the ribs following two orthogonal X and Y planes

Next, we drove cavitation experiments in degassed water to qualitatively study the three-dimensional position shape of the cavitation cloud after the ribs' aberration. Based on [4], we fixed n_t at 10 volumes for an effective cavitation map volume rate of 10 Hz. Figure 3 shows the cavitation power signal displayed on two orthogonal X and Y planes of an acquired volume while histotripsy. Table 1 shows the width, length and cavitation cloud centroid position in relation to the central axis of the image, which we assume corresponds to the central axis of the transducer.

Table 1 - Three-dimensional dimensions of the cavitation cloud and distance to the central axis of the transducer, using 3D coherent passive cavitation imaging. $N = 80$

Measure	X plane	Y plane
Width (cm)	1.34 ± 0.1	1.3 ± 0.1
Length (cm)	1.6 ± 0.08	1.54 ± 0.13
Distance to the central axis of the transducer (cm)	0.18 ± 0.02	0.01 ± 0.01

The cavitation cloud centroid remains centred around the central axis of the image, but a slight displacement of about 2 mm in the X plane and less than 0.2 mm in the Y plane was found.

Moreover, we can observe that the bubble cloud is roughly symmetrical in the X and Y planes with a width around 1.3 cm and a length around 1.6 cm, and the shape of the cloud remains roughly spherical.

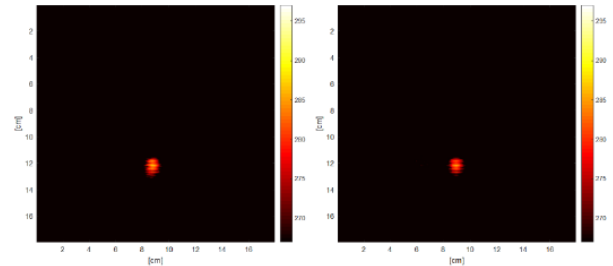


Figure 3 - 3D passive cavitation map while histotripsy through human ribs in degassed water. Left: Plane X = 128/256. Right: Plane Y = 128/256

We then conducted cavitation experiments in degassed water with an estimated minimal focal pressure peak value under -18 MPa, well above the cavitation threshold. Figure 4 shows examples of orthogonal X and Y planes during histotripsy. In the X planes, we can observe the apparition of a secondary cavitation cloud at about -10 dB pointed by a blue arrow (while the mean cloud appears at about -5 -dB). Yet, the secondary cloud is absent in the Y plane. The secondary cloud is quickly driven by the ultrasound path and fuses with the main cavitation cloud and the main cavitation cloud shape and size are altered.

Indeed, the secondary cavitation cloud happens to be off centre, completely outside the Y plane. We can imagine that 2D imaging would be limiting in such a case. Furthermore, the 3D rendering shows us that there is only one secondary cavitation cloud.

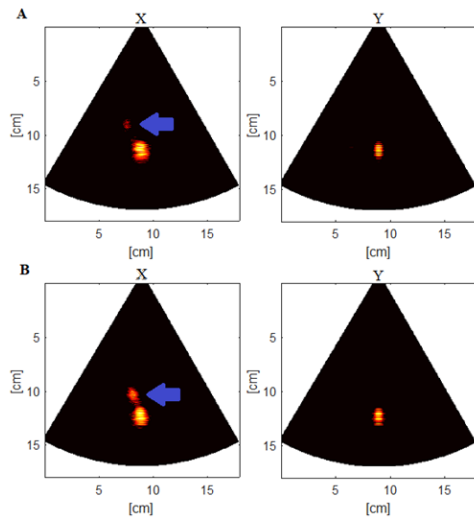


Figure 4 – 3D passive cavitation map while histotripsy through human ribs in water. Left: Plane $X = 128/256$. We can observe a second cavitation cloud (blue arrow). Right: Plane $Y = 128/256$

3D imaging allows to cover a whole volume where cavitation can occur, enabling a safer monitoring of the histotripsy procedure. It gives full information to visualize the complete shape of the bubble cloud and a complete assessment of the bubble cloud impact range.

IV. DISCUSSION AND CONCLUSION

We have already demonstrated the feasibility of volumetric coherent passive cavitation imaging as the algorithms are easily transposed to 3D applications [4]. 3D passive cavitation imaging could increase the safety of the treatment monitoring as the whole bubble cloud could be precisely located within a volume, even if both therapy and imaging transducers present misalignments.

To this day, the effects of aberrating mediums such as of the ribcage the skull have been widely explored on HIFU emissions [6], especially attenuation, the decrease on the necrosis efficacy and misfiring, and aberration correction solutions using for example adaptive focusing have been proposed [7]. For histotripsy through the ribcage, nevertheless, some studies have already shown that there is no strict need for aberration correction [8]. It should be noted that we assume that strong aberrations affect mainly the therapeutic beam due to the large aperture of the therapeutic transducer, whereas the imaging probe has a limited dimension and is located in an intercostal space with no ribs on the ultrasound path.

Furthermore, in water and in simple and homogenic mediums, the cavitation cloud is mainly symmetrical with an oval or circular shape, and 2D imaging gives enough information of the cloud dynamics, shape and position. Yet, in more complex mediums (c.f. *in vivo*) and in mediums presenting strong interfaces (c.f. the ribs, calcifications), the bubble cloud shape and size may vary asymmetrically.

In fact, 2D imaging may be limited in a medium with strong aberrations that may displace the therapeutic focal spot outside the imaging plane. As the cavitation cloud shape may be

asymmetrical, and secondary cavitation clouds may appear, 3D cavitation imaging may overcome 2D imaging limitations. Our results highlighted the need of a 3D real-time monitoring technique with good contrast to ensure that no adverse effects arrive such as secondary cavitation clouds.

A limitation of the study is the use of high channel count electronics for full 3D imaging, which are complex and expensive and remain limited for clinical applications [9]. Nevertheless, this approach could be implemented on 3D ultrasound systems with micro beamformers. At this day, clinical 3D cardiac imaging systems exist (General Electric©, Philips©), and cavitation imaging could be implemented in those systems. Despite its great potential, today 3D imaging is mostly seen as complementary to 2D imaging in routine practice. The visualization and the interpretation of a full 3D volume while histotripsy may remain long and complicated, and ergonomic tests as well as the reaction time measure should be driven.

ACKNOWLEDGMENTS

The project was supported by Cardiawave SA, the ANR-10-IDEX-0001-02 PSL* Research University and the ANR-17-CE19-0019 "Valvosoft". This project has received funding from the European Union's Horizon 2020 research and innovation programme under grant agreement No 829492.

REFERENCES

- [1] Villemain, Olivier, Justine Robin, Alain Bel, Wojciech Kwiecinski, Patrick Bruneval, Bastien Arnal, Mathieu Rémond, Mickael Tanter, Emmanuel Messas, and Mathieu Pernot. "Pulsed Cavitation Ultrasound Softening: A New Noninvasive Therapeutic Approach for Calcified Bioprosthetic Valve Stenosis." *JACC: Basic to Translational Science* 2, no. 4 (August 1, 2017): 372–83.
- [2] Khokhlova, VA, JB Fowlkes, WW Roberts, GR Schade, Z Xu, TD Khokhlova, TL Hall, AD Maxwell, YN Wang, and CA Cain. "Histotripsy Methods in Mechanical Disintegration of Tissue: Toward Clinical Applications." *International Journal of Hyperthermia: The Official Journal of European Society for Hyperthermic Oncology, North American Hyperthermia Group* 31, no. 2 (March 2015): 145–62.
- [3] Coviello, Christian, Richard Kozick, James Choi, Miklós Gyöngy, Carl Jensen, Penny Probert Smith, and Constantin-C. Coussios. "Passive Acoustic Mapping Utilizing Optimal Beamforming in Ultrasound Therapy Monitoring." *The Journal of the Acoustical Society of America* 137, no. 5 (May 2015): 2573–85.
- [4] Daniel Suarez Escudero, Guillaume Goudot, Michael Vion, Mickael Tanter, and Mathieu Pernot. "2D and 3D Real-Time Passive Cavitation Imaging of Pulsed Cavitation Ultrasound Therapy in Moving Tissues." *Physics in Medicine & Biology* 63, no. 23 (December 6, 2018): 235028.
- [5] Provost, Jean, Clement Papadacci, Juan Esteban Arango, Marion Imbault, Mathias Fink, Jean-Luc Gennisson, Mickael Tanter, and Mathieu Pernot. "3D ultrafast ultrasound imaging *In Vivo*." *Physics in Medicine and Biology* 59, no. 19 (October 7, 2014): L1–13.
- [6] Li, Faqi. "Effect of ribs in HIFU beam path on formation of coagulative necrosis in goat liver." In *AIP Conference Proceedings*, 829:477–80. Boston, Massachusetts (USA): AIP, 2006.
- [7] Cochar, E., J. F. Aubry, M. Tanter, and C. Prada. "Adaptive projection method applied to three-dimensional ultrasound focusing and steering through the ribs." *The Journal of the Acoustical Society of America* 130, no. 2 (August 2011): 716–23. <https://doi.org/10.1121/1.3607419>.
- [8] [Kim, Y, E Vlaisavljevich, G E Owens, S P Allen, C A Cain, and Z Xu. "In Vivo transcatheter histotripsy therapy without aberration correction." *Physics in Medicine and Biology* 59, no. 11 (June 7, 2014): 2553–68.
- [9] Wu, Victor Chien-Chia, and Masaaki Takeuchi. "Three-dimensional echocardiography: current status and real-life applications." *Acta Cardiol Sin*, n.d., 12. (2017)